High-pressure structural transformations of Sn up to 138 GPa: Angle-dispersive synchrotron x-ray diffraction study

Ashkan Salamat,[1,2,*] Richard Briggs,[3,4] Pierre Bouvier,[5] Sylvain Petitgirard,[2] Agnès Dewaele,[6] Melissa E. Cutler,[3,7] Furio Corà,[3] Dominik Daisenberger,[3,8] Gaston Garbarino,[2] and Paul F. McMillan[3,†]

[1]*Lyman Laboratory of Physics, Harvard University, Cambridge, Massachusetts 02138, USA*

[2]*European Synchrotron Radiation Facility, Boîte Postale 220, 38043 Grenoble Cedex, France*

[3]*Chemistry and Institute of Shock Physics, University College London, 20 Gordon Street, London WC1H 0AJ, United Kingdom*

[4]*SUPA, School of Physics and Astronomy, Centre for Science at Extreme Conditions, The University of Edinburgh, Edinburgh, United Kingdom*

[5]*Laboratoire des Matériaux et du Génie Physique, CNRS, Grenoble Institute of Technology, 3 Parvis Louis Néel, 38016 Grenoble, France*

[6]*CEA/DAM/DIF, F-91297 Arpajon, France*

[7]*Materials Modelling Group, Atomic Weapons Establishment, Aldermaston, Reading RG7 4PR, United Kingdom*

[8]*Diamond Light Source Ltd., Diamond House, Harwell Science Campus, Didcot, Oxfordshire OX11 0DE, United Kingdom*

(Received 28 May 2013; revised manuscript received 23 July 2013; published 9 September 2013)

The high-pressure behavior of elemental Sn has been studied by angle-dispersive synchrotron x-ray diffraction up to 138 GPa under quasihydrostatic conditions at room temperature. The data confirm the occurrence of a first-order phase transition at 10.8 GPa between β-Sn (Sn-II) ($I4_1/amd$) and a further body-centered-tetragonal polymorph (γ-Sn or Sn-III) ($I4/mmm$). Above 32 GPa, this phase exhibits a distortion into a new body-centered-orthorhombic (bco) modification ($Immm$). Beyond 70 GPa, the structure becomes body-centered cubic (bcc) (Im-$3m$). There is a region of coexistence where the bcc reflections are observed to appear superimposed on the bco pattern above 40 GPa and the two diffraction signatures coexist until 70 GPa. We examined this possible existence of a kinetically hindered first-order phase transition between the two polymorphs by performing density functional theory (DFT) calculations with an emphasis on the potential energy in response to axial (c/a,b/a) distortions at constant volume. The DFT results suggest a slightly different interpretation of the structural transformations. At low pressure, the global minimum energy is always centered around $b/a = 1$, and there is no indication of transformation to a bco structure. However, any small strains in the c/a ratio in the system would provide an orthorhombic distortion of the observed magnitude. Such strains could be induced due to slight deviations from hydrostatic conditions in the experimental study. Concerning the possible bco-bcc phase transitions, the DFT calculations reveal an energy surface with a barrier developed between solutions with different c/a values over the pressure range of interest. Crucially, the calculated barrier heights are low, and they disappear in the region of the observed phase transformation. The DFT results indicate a mechanically softened material that may exhibit localized domain structures in response to even slightly nonhydrostatic stress conditions.

DOI: 10.1103/PhysRevB.88.104104 PACS number(s): 62.50.−p, 31.15.A−, 61.50.Ks

I. INTRODUCTION

Sn lies at a boundary in the periodic table between the semiconducting group-14 elements Si and Ge and the heavier metallic member Pb where d orbital participation along with spin-orbit coupling and relativistic effects play a significant role in the bonding.[1] Both Si and Ge are well known to undergo a complex series of phase transitions between various metallic polymorphs as pressure is increased,[2–6] whereas, the phase diagram of Pb is found to be much simpler.[7,8] Below 286 K, Sn exists in its diamond-structured α-Sn phase (Sn-I with Fd-$3m$ symmetry), similar to Si, Ge, and C diamond.[9] At ambient pressure and temperature, the metallic β-Sn phase has a body-centered-tetragonal (bct) structure ($I4_1/amd$). Near 10 GPa, an early high-pressure study indicated a phase transition occurred into a body-centered-cubic (bcc) form that became known as γ-Sn or the Sn-III polymorph.[10] Barnett *et al.* later noted that the polymorph formed above 9.5 GPa had a tetragonally distorted structure ($I4/mmm$), which is bct with a c/a axial ratio of $\sim$0.91.[11] In studies carried out with increasing pressure, it was observed that the axial ratio increased and that new reflections indicating the presence of a bcc structure (Im-$3m$) appeared in the x-ray-diffraction pattern above $P \sim 44$ GPa.[2,12] These authors noted a wide coexistence range between the bct ($I4/mmm$) and the bcc (Im-$3m$) phases extending between 40 and 56 GPa. Desgreniers *et al.* carried out energy-dispersive x-ray-diffraction experiments between 52 and 120 GPa and found evidence for only the bcc (Im-$3m$) structure.[13] This polymorph remained stable up to 157 GPa where it was recently shown to transform into a hcp-Sn ($P6_3/mmc$) structure in agreement with theoretical predictions.[14,15] There is renewed interest in the anomalous polymorphic behavior of Sn in the 40–70 GPa range due to recent melting studies of this important material that reveal some unusual features.[16–18]

Electronic structure calculations to understand the unusual polymorphic behavior of Sn during compression were first performed by Christensen[19] and Christensen and Methfessel.[20] Their papers identified the stability of the bct phase at low pressure due to a Jahn-Teller-like distortion, associated with an electronic band near the Fermi energy at the Brillouin-zone boundary, and the emergence of a secondary minimum at $c/a = 1$, corresponding to a bcc solution in the

potential-energy curve, that became stabilized as the cubic structure at high pressure. The conclusion from that paper was that the bct-bcc transformation was, indeed, first order in nature.

Here we have applied a combined experimental and theoretical approach to understand the nature of this deceptively simple elemental system. We investigated the polymorphism of Sn up to 138 GPa using high-resolution angular dispersive x-ray diffraction (ADXRD) techniques in a diamond-anvil cell (DAC) using pressurization conditions designed to provide quasi- to near-hydrostatic compression to the sample. We also apply advanced density functional theory (DFT) techniques to model the structural and electronic properties of Sn with a special emphasis on the energetics of axial distortions occurring among the body-centered structural polymorphs. Our experimental work identifies and discusses the formation of a new body-centered orthorhombic [(bco): $Immm$] phase observed above 32 GPa and places new constraints on the coexistence of this structural polymorph with the bcc phase observed at a higher pressure. The DFT results yield new insights into how these structures are formed as a result of electronic instabilities developed within this unusual element with its intermediate bonding characteristics at high pressure. The studies also highlight general aspects of combining experimental and theoretical approaches to understand such structural phase transformations.

II. EXPERIMENTAL AND THEORETICAL METHODS

High-pressure experiments were conducted using membrane-driven DACs with the polycrystalline Sn sample (99.9%, Merck) analyzed using ADXRD at the high-pressure beamline ID27 (ESRF). A monochromatic incident beam (33 keV, $\lambda = 0.3738$ Å) was focused down to a FWHM of 1.7×2.3 μm. Data were collected using either a MarCCD 165 detector or a Mar345 image plate. Four compression runs were carried out at ambient temperature using either He (three runs) or Ne (one run) as the pressure-transmitting medium (PTM). W (99.9%, Goodfellow) and SrB_4O_7:Sm^{2+} were used as pressure indicators.[21,22] Pressures were determined and were cited in this paper using the Vinet equation of state (EOS) using W as an internal standard with $K_0 = 296$ GPa and $K_0' = 4.3$.[21] Diamond culet sizes of 300, 200, 150, and 100 μm were selected to attain final pressures of 65, 81, 105, and 138 GPa, respectively. Re gaskets were indented relative to the culet size and were drilled using a pulsed Nd^{3+}:YAG laser. Interferometry was used to ensure that sample size and indent depth were of the correct relative dimensions to prevent the sample bridging the diamond culets.

ADXRD data were analyzed using FIT2D,[23] CRYSFIRE,[24] DATLAB,[25] and EXPGUI GSAS.[26] In the loading with the 100-μm culet diamonds, the sample gave quasi-single-crystal diffraction, here, diffraction spots were analyzed individually.

Constant pressure and constant volume DFT calculations were performed with the CASTEP code[27] using plane-wave basis sets and the Perdew-Burke-Ernzerhof generalized gradient approximation (GGA) exchange-correlation functional.[28] We used a small-core pseudopotential that treats the Sn 4d electrons as valence states and a plane-wave cutoff energy of 479 eV that was optimized in preliminary runs. Reciprocal space integrations were performed using a Monkhorst-Pack grid[29] of $26 \times 26 \times 26$ k points. Constant volume geometry optimizations were carried out to investigate the effect on the potential-energy surface (PES) of variations from the underlying bcc Sn structure as a function of the unit-cell volume and its axial c/a and b/a strain parameters. We considered cell volumes ranging between 28 and 16 Å^3, that corresponded to pressures between approximately -0.5 and 97.6 GPa, determined from our DFT runs carried out under constant P conditions. At each volume, a grid of 546 calculations was performed, varying the c/a ratio between 0.80 and 1.25 and the b/a ratio between 0.99 and 1.01 with step sizes selected to provide the necessary energy resolution. The structural transformations then were also studied using constant pressure optimizations in the range of $P = 0$–100 GPa with 5-GPa steps. These were initiated from three different starting configurations with axial ratios of 1.1:1:0.9, 1.01:1:0.9, and 1.01:1:0.99 to model the approach to a global minimum structure at each pressure.

III. RESULTS AND DISCUSSION

A. Experimental observations

The stability field for the β-Sn phase with a body-centered-tetragonal ($I4_1/amd$) structure extends up to 10.8 GPa at room temperature where it transforms into a different body-centered-tetragonal ($I4/mmm$) phase (Fig. 1). The two phases are

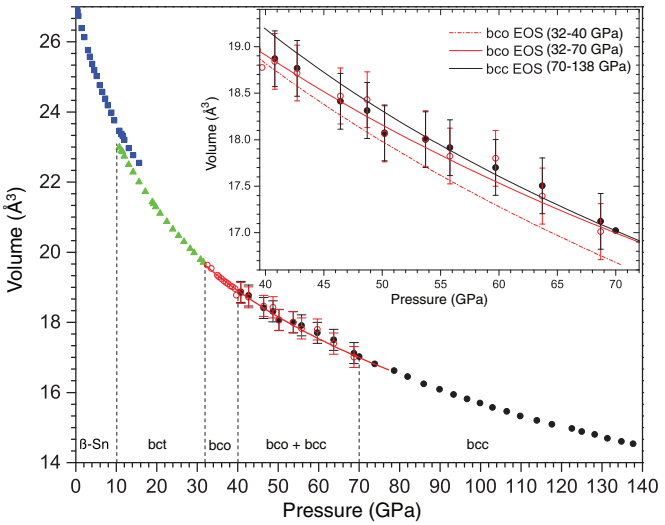

FIG. 1. (Color online) The volume-pressure relations of Sn up to 138 GPa at room temperature using He as a pressure-transmitting medium. The β-Sn polymorph is stable below 10.8 GPa and coexists metastably with the body-centered-tetragonal (bct $I4/mmm$) phase up to 15.7 GPa. An orthorhombic distortion is observed above 32 GPa, leading to a bco structure ($Immm$). Coexistence of bco ($Immm$) and bcc (Im-$3m$) structure types is visible in the x-ray-diffraction patterns between 40 and 70 GPa. Throughout this range, the volumes determined for the bco and bcc phases do not fit the third-order Birch-Murnaghan equation of state well (see the inset). Two different EOS fits are shown for the bco ($Immm$) phase, one before (32–40 GPa) and a second leading up to and extending throughout (32–70 GPa) the region of coexistence range. Above 70 GPa, only the bcc (Im-$3m$) polymorph is observed.

linked by a first-order transformation, and they are observed to coexist metastably up to 15.7 GPa. The volume reduction between the β-Sn ($I4_1/amd$) and the bct ($I4/mmm$) phases at 10.8 GPa is approximately 2%. Liu and Lui previously reported the onset of the bct ($I4/mmm$) phase at 9.7 GPa with a smaller region of coexistence up to 10.3 GPa.[12]

Above 15.7 GPa, the diffraction data are initially fit well by Le Bail refinement using a bct ($I4/mmm$) structure solution (wR_p and R_p values are 1.01% and 0.64%, respectively). The c/a ratio is observed to increase slightly between 0.912 and 0.934 with increasing pressure. However, above 32 GPa, the patterns can no longer be fit precisely (wR_p and R_p values are 3.72% and 3.54%, respectively) using this structure model, and the data indicate the presence of an orthorhombic distortion (wR_p and R_p values are 1.75% and 1.55%, respectively, within space group $Immm$). The main deviation from the tetragonal constraint appears for the 101, 200, and 211 reflections of an ideal $I4/mmm$ structure as would be expected through the lowering of symmetry to an orthorhombic crystal structure and, consequently, the loss of the -4 rotation axis. To illustrate the change in symmetry, the FWHM for several reflections was plotted throughout the pressure range (Fig. 2). The incipient splitting of the 200 and 211 reflections is clearly evident compared to the 002 and 112 reflections that are not affected by the reduction in symmetry. These data from the experimental x-ray-diffraction patterns might indicate the occurrence of a second-order phase transition between the bct ($I4/mmm$) and the bco ($Immm$) polymorphs.

We conducted our experiments using both He and Ne as the PTM. Helium crystallizes at 12 GPa at ambient temperature

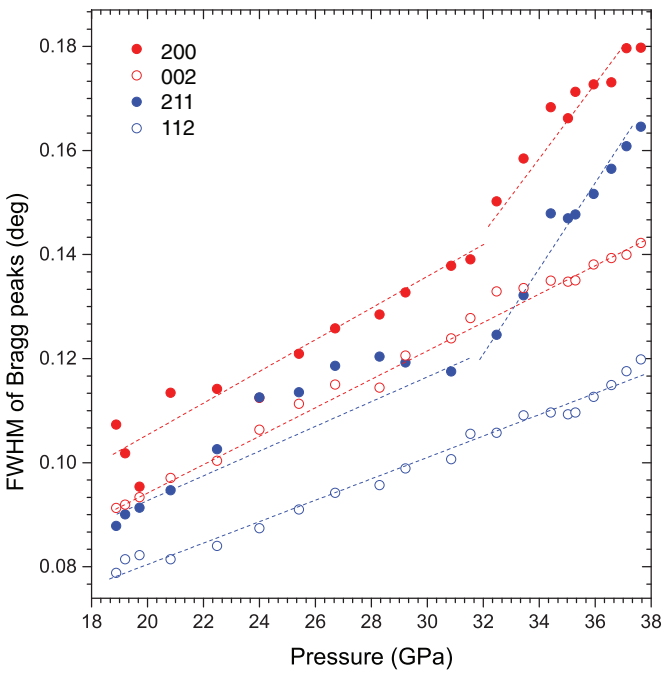

FIG. 2. (Color online) Full width at half maximum analysis of Bragg peaks of Sn up to $P \sim 38$ GPa using a He pressure-transmitting medium. A sharp increase in FWHM is observed for the 200 and 211 reflections, whereas, the 002 and 112 reflections remain linear. This is indicative of the system lowering symmetry from body-centered tetragonal ($I4/mmm$) to body-centered orthorhombic ($Immm$).

but is found to provide quasihydrostatic conditions over a wide compression range.[30–33] Some compression studies using He have shown evidence for nonhydrostatic stresses developed within the sample above 30 GPa, but this remains very small with a standard deviation in pressure measurements throughout the cell of only 0.3–0.5% at 150 GPa.[31,34] Neon crystallizes at a lower pressure (4 GPa) and is expected to provide less hydrostatic compression conditions over a wider pressure range. Crucially, for this study, the onset of the orthorhombic (bco) distortion was observed to occur at the same pressure (32 GPa) using both He and Ne as PTM environments.

Following compression to 40 GPa, the x-ray-diffraction data clearly show the appearance of additional peaks due to a cubic (bcc) phase, and both the bco and the bcc reflections remain present within the pattern until 70 GPa with relative weights that change continuously throughout the pressure range. That surprising result could indicate the presence of a first-order phase transformation between the bco and the bcc polymorphs, kinetically hindered by a high energetic barrier. That scenario was initially proposed by Christensen following early calculations to study Sn behavior at high pressure.[19] Our new DFT results described below provide a more complete view of the structural transformation properties in this pressure range.

The high quality of our x-ray data sets (Fig. 3) permitted us to carry out a detailed analysis of the diffraction signature throughout the coexistence range. The unusual behavior of the bcc polymorph first attracted our attention. In one of our experiments, the diffraction data revealed the sample to be quasisingle crystalline (Fig. 4) in nature, and we were able to integrate each diffraction spot individually to extrapolate volumes for the bcc polymorph according to different crystallographic planes (Fig. 5). The system did not behave as expected for a strain-free cubic phase. Between

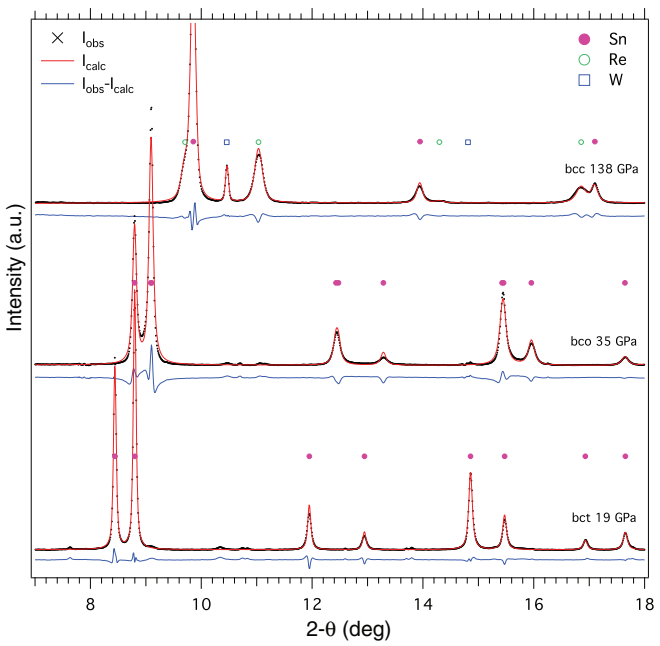

FIG. 3. (Color online) Rietveld refinements of x-ray-diffraction patterns collected at 19, 35, and 138 GPa representing the bct, bco, and bcc phases of Sn (closed circles). ($\lambda = 0.3738$ Å.)

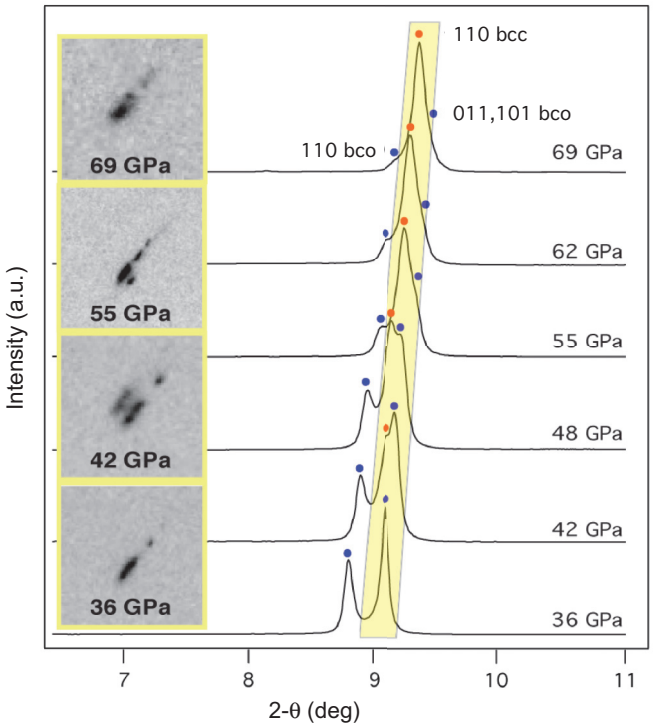

FIG. 4. (Color online) Details of x-ray-diffraction data around the position of the 110 reflection obtained throughout the 36–69-GPa coexistence range between bco ($Immm$) and bcc (Im-$3m$) structures. The image plate data (left) show only a single bco ($Immm$) structure at 36 GPa with the clear onset of a bcc (Im-$3m$) structure with the same grain structure and common axial parameters indicated by the shape of the spots at 42 GPa. As the pressure is raised to 55 GPa, the bco ($Immm$) reflections begin to disappear, and only the bcc (Im-$3m$) structure remains by 69 GPa. The results are summarized in the integrated data plot shown on the right. ($\lambda = 0.3738$ Å.)

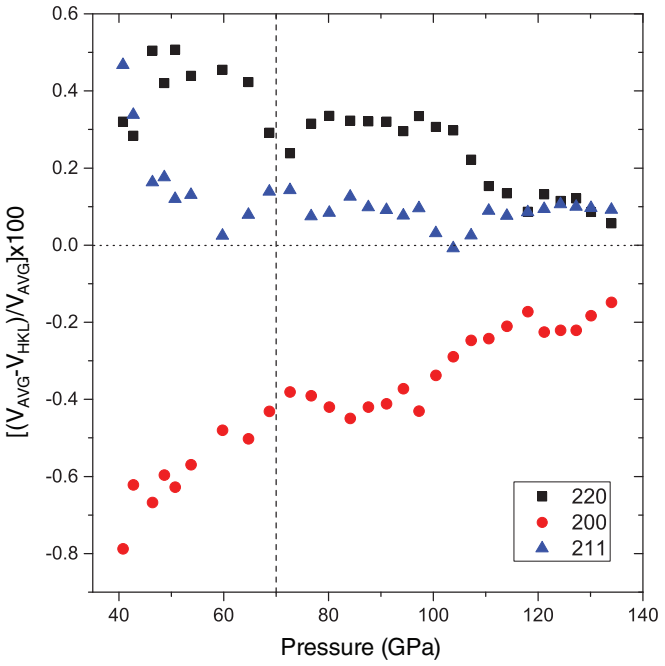

FIG. 5. (Color online) The difference plot of the volume from the equation of state for the body-centered-cubic (Im-$3m$) phase and the volume obtained from different Bragg peaks. For the pressure range of 40–70 GPa, there is coexistence with a body-centered-orthorhombic phase, beyond 70 GPa only the bcc phase remains.

10 and 32 GPa, the $V(P)$ relation could be fit well by a Birch-Murnaghan (BM) relation expanded to third order, and this could be extended with similar accuracy to 40 GPa by taking account of the bco distortion (Fig. 1). Above 70 GPa, the BM relation provided an excellent fit to the EOS for the bcc form. However, at intermediate pressures, the EOS behaved badly. First, it was not possible to define a unique value for the volume of the bcc phase throughout the coexistence region as different reflections gave rise to different results. Those are shown as error bars on the $V(P)$ plot shown in Fig. 1. Next, extensions of the EOS "upwards" from the bco phase or "downwards" from the bcc polymorph stable above $P > 70$ GPa cannot be used to match the experimental $V(P)$ relations within the transformation zone (see inset to Fig. 1). That result indicates that both the bcc and the bco structures coexisting within the transformation range between 40 and 70 GPa are experiencing nonisotropic strains.

Another interesting feature emerges from close inspection of the two-dimensional diffraction images as the single-crystal reflections evolve throughout the 40–70-GPa range (Fig. 4). The new peaks indicating the first appearance of the cubic (Im-$3m$) structure are recorded at the same azimuthal position as the parent bco ($Immm$) phase, indicating that the overall crystal retains its orientation throughout the transformation. The azimuthal width of the bcc (Im-$3m$) single-crystal peak is larger than that of the parent bco ($Immm$), suggesting crystallographic defects must be present in the new structure. No change in the bcc vs bco peak intensity ratios were observed in data taken at different positions within the sample, indicating that the bcc (Im-$3m$) structure has emerged as oriented microdomains within and coherent with the parent bco ($Immm$) matrix.

In order to extract elastic parameter data, we fitted the experimental $V(P)$ relations of the β-Sn, bct, bco, and bcc structures to a third-order Birch-Murnaghan EOS (BM-3) for each phase within its stability field.[35–38] Directly fitting the data allowed us to obtain a preliminary set of K_P, K'_P, and V_P parameters where P is an appropriate reference pressure for each structural polymorph. We neglected data points lying at the extreme limits of the metastable coexistence ranges (Fig. 6). Using this procedure, the β-Sn ($I4_1/amd$) phase was fitted between 0.2 and 9.8 GPa, the bct ($I4/mmm$) polymorph was fitted from 15.6 to 31.1 GPa, the bco ($Immm$) distorted structure was fitted from 32 to 40 GPa, and the bcc (Im-$3m$) phase stable at high pressure was fitted from 70 to 138 GPa. The values were then refined using a linearized version of the BM-3 relation involving reduced Eulerian strain (f) and applied stress (F) variables[39] defined by

$$F = P[3f(1+2f)^{5/2}]^{-1}, \tag{1}$$

$$f = \frac{1}{2}\left[\left(\frac{V_0}{V}\right)^{2/3} - 1\right]. \tag{2}$$

In this analysis, V_P was treated as an adjustable parameter, the bulk modulus K_P is derived from the intercept of the linear

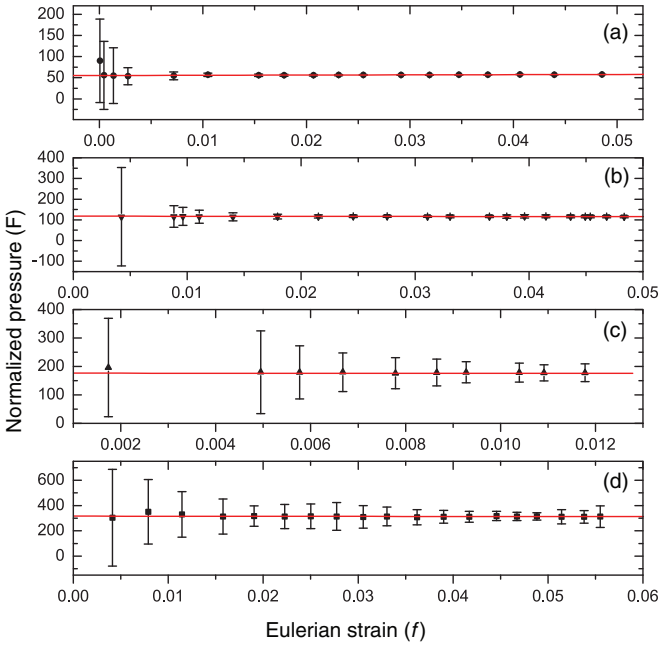

FIG. 6. (Color online) Normalized pressure (F) vs Eulerian strain (f). All values are given in Table I and are calculated for when only a single phase is present and He is used as the pressure-transmitting medium: (a) β-Sn ($I4_1/amd$) up to 10.8 GPa, (b) bct ($I4/mmm$) from 15.6–31 GPa, (c) bco ($Immm$) from 32–40 GPa, and (d) bcc (Im-$3m$) from 70–138 GPa.

relation with the y axis, and its first pressure derivative K'_p is linearly related to the slope of the F-f relation (Fig. 6). Using this procedure, the intercept of the linearized relation could be extrapolated back to zero pressure to define hypothetical values of V_0, K_0, and K'_0 for the three structural polymorphs and to allow comparison of their elastic properties at the same reference pressure. The elastic constant information derived from experimental data obtained using He as the PTM is summarized in Table I. In this table, we also included V_0, K_0, and K'_0 values obtained from our DFT calculations. That comparison is valuable because the theoretical model could be examined metastably to zero-pressure conditions, providing reference values for K_0 and K'_0 directly, unlike the experimental data sets that could only be obtained by extrapolation. We note that only a single $V(P)$ curve exists from the DFT data because the three structures are related by distortions in the c/a or b/a lattice parameters at constant volume. The static DFT calculations were carried out at $T =$ 0 K for an infinite crystal under periodic boundary conditions, whereas, the experiments were conducted at $T = 300$ K for polycrystalline samples that could spontaneously develop domain structures. These points are discussed in detail below.

Our experimental study, thus, confirms or reveals several fascinating findings about the behavior of elemental Sn throughout the 10–130-GPa range. There is a new possible second-order phase transition between bct and bco forms of γ-Sn (Sn-III), followed by a potential first-order transformation between bco and bcc polymorphs that is kinetically hindered at ambient temperature. However, the bco distortion occurs at the limit of our experimental resolution, and it could be associated with slightly nonhydrostatic compression conditions developed within the polycrystalline sample. The role of such effects must be examined. The second (bco-bcc) major transformation event also appears to involve considerable nonisotropic strains among the phases coexisting within the sample. For these reasons, we undertook a parallel study of the high-pressure behavior of Sn throughout this pressurization regime using contemporary DFT methods (see Table II).

TABLE I. Summary of bulk modulus values for Sn recorded using He as a pressure-transmitting medium. Two sets of compressibility values are given, both fitted linearly using normalized pressure (F) vs Eulerian strain (f). The first set consists of K_P (GPa) and K'_P values for V_P when $P = 0$, whereas, the second set consists of values given at the transition pressure P for each phase and for when only the single phase is present. DFT GGA values for elastic parameters from BM-3 analysis of the single $V(P)$ compression curve obtained for all phases at $T = 0$ K referenced to zero pressure are included for comparison.

Phase	P (GPa)	V_P (Å^3)	K_P (GPa)	K'_P
β-Sn ($I4_1/amd$)	0	27.06(1)	54.7(5)	4.5(1)
bct ($I4/mmm$)	0	26.25(2)	62(3)	4.0(1)
	15.6	22.00(4)	118(3)	3.7(2)
bco ($Immm$)	0	26.2(1)	63(2)	4.0(1)
	32	19.63(8)	176(4)	3.5(5)
bcc (Im-$3m$)	0	24.5(3)	92(4)	4.0(1)
	70	17.02(2)	316(5)	3.9(2)
DFT (all phases)	0	27.74	45.9	4.8

B. DFT studies

Studies of Sn polymorphism throughout the intermediate-pressure range where bct (bco) and bcc phases are reported to coexist were carried out by Christensen and Methfessel using a linear muffin-tin orbital method.[20] Those studies investigated the energetics associated with c/a distortions within bct/bcc structures and reported results for pressures indicated to correspond to 0, 10, and 50 GPa, although no EOS data were published. At low P, constant volume calculations indicated an anharmonic potential function around a minimum value near $c/a = 0.9$, corresponding to the bct structure observed experimentally. The c/a value increased slightly with increasing pressure as also observed experimentally, and a subsidiary minimum was seen to be present in the potential-energy function near $c/a = 1$ that signaled the emergence of another polymorph with bcc symmetry. This was initially metastable but became stabilized at high pressure. In an intermediate-pressure range, the calculation showing two minima indicated an energy barrier between them, and this led Christensen[19] to propose the presence of a first-order phase transition between the bct and the bcc polymorphs, that could give rise to their experimentally observed coexistence during ambient temperature compression experiments. The calculations indicated the appearance of the bcc phase was due to a Jahn-Teller-like splitting of H_{15} electronic states near the Fermi level at the Brillouin-zone boundary.

Our new results using modern DFT methods provide a more complete picture that helps us understand the experimental findings. We first examined the variation in potential energy

TABLE II. The unit-cell parameters of the high-pressure phases of Sn at ambient temperature. All values are given using He as the pressure-transmitting medium, and pressures are determined with W as the pressure marker.[21]

Phase	Pressure (GPa)	a (Å)	c (Å)	c/a ratio	Volume (per atom) (Å^3)	Phase	Pressure GPa	a (Å)	b (Å)	c (Å)	Volume (per atom) (Å^3)
β	0.2	5.8259(3)	3.1776(2)	0.54543	26.96(1)	bco	32.5	3.469(2)	3.482(2)	3.250(1)	19.64(1)
β	0.2	5.8256(4)	3.1774(2)	0.54542	26.95(1)	bco	33.4	3.462(2)	3.476(2)	3.246(1)	19.54(1)
β	0.3	5.8235(3)	3.1760(2)	0.54538	26.92(1)	bco	35.0	3.449(2)	3.463(2)	3.239(1)	19.35(1)
β	0.4	5.8184(4)	3.1729(3)	0.54531	26.85(2)	bco	35.3	3.448(1)	3.458(2)	3.2371(8)	19.301(7)
β	0.7	5.8107(4)	3.1680(2)	0.54521	26.74(1)	bco	35.9	3.444(3)	3.456(3)	3.234(1)	19.25(1)
β	1.4	5.7863(4)	3.1531(2)	0.54493	26.39(1)	bco	36.5	3.436(3)	3.453(3)	3.234(2)	19.19(1)
β	2.1	5.7682(5)	3.1421(2)	0.54473	26.13(2)	bco	37.1	3.434(3)	3.451(3)	3.230(2)	19.14(2)
β	3.0	5.7416(4)	3.1262(3)	0.54447	25.76(1)	bco	37.6	3.430(3)	3.448(3)	3.231(2)	19.1(2)
β	3.5	5.7285(5)	3.1183(3)	0.54435	25.58(2)	bco	38.2	3.426(2)	3.443(2)	3.228(1)	19.04(1)
β	4.1	5.7132(3)	3.1093(3)	0.54422	25.37(1)	bco	38.7	3.425(2)	3.439(2)	3.228(1)	19.01(1)
β	4.6	5.7003(6)	3.1017(3)	0.54413	25.19(3)	bco	39.3	3.421(3)	3.436(3)	3.227(1)	18.96(2)
β	5.1	5.6879(5)	3.0943(6)	0.54401	25.02(4)	bco	39.7	3.425(3)	3.407(3)	3.218(2)	18.78(2)
β	5.9	5.6690(1)	3.0830(7)	0.54386	24.76(3)	bco	40.8	3.419(4)	3.418(4)	3.224(3)	18.84(2)
β	6.5	5.6543(9)	3.0747(9)	0.54378	24.58(7)	bco	42.7	3.406(4)	3.401(4)	3.232(3)	18.72(2)
β	7.2	5.6397(5)	3.0662(5)	0.54368	24.38(4)	bco	46.4	3.381(5)	3.376(4)	3.236(2)	18.47(3)
β	7.9	5.6253(6)	3.0578(5)	0.54358	24.19(6)	bco	48.7	3.379(4)	3.371(4)	3.235(2)	18.43(2)
β	8.8	5.6096(5)	3.0487(4)	0.54348	23.98(5)	bco	50.2	3.344(5)	3.341(4)	3.234(3)	18.06(3)
β	9.5	5.5927(8)	3.0390(6)	0.54339	23.76(7)	bco	53.7	3.331(4)	3.329(4)	3.248(3)	18.01(2)
β	10.8	5.569(6)	3.0267(6)	0.54326	23.46(5)	bco	55.8	3.299(5)	3.286(5)	3.288(3)	17.82(3)
β	11.3	5.563(9)	3.022(8)	0.5432	23.38(9)	bco	59.7	3.286(5)	3.281(5)	3.301(4)	17.8(3)
β	11.5	5.559(1)	3.020(8)	0.5432	23.33(8)	bco	63.7	3.269(4)	3.265(4)	3.258(2)	17.39(2)
β	12.0	5.549(1)	3.014(1)	0.5432	23.21(7)	bco	68.7	3.253(5)	3.247(5)	3.222(3)	17.01(3)
β	13.1	5.531(3)	3.004(3)	0.5431	22.97(8)	bcc	40.8	3.354(5)			18.90(1)
β	14.1	5.515(7)	2.994(6)	0.5429	22.74(8)	bcc	42.7	3.348(1)			18.77(5)
β	15.6	5.480(2)	3.000(2)	0.5472	22.55(7)	bcc	46.4	3.326(1)			18.41(5)
bct	10.8	3.694(3)	3.370(4)	0.9124	22.99(9)	bcc	48.7	3.320(3)			18.31(8)
bct	11.3	3.688(1)	3.366(2)	0.9127	22.89(8)	bcc	50.2	3.306(4)			18.0(1)
bct	11.5	3.686(3)	3.366(3)	0.9132	22.87(2)	bcc	53.7	3.302(5)			18.0(1)
bct	12.0	3.678(8)	3.362(9)	0.9140	22.74(8)	bcc	55.8	3.297(3)			17.91(9)
bct	13.1	3.663(4)	3.354(6)	0.9156	22.50(3)	bcc	59.7	3.283(3)			17.70(9)
bct	14.1	3.649(4)	3.347(6)	0.9172	22.28(3)	bcc	63.7	3.271(5)			17.5(1)
bct	15.6	3.631(6)	3.337(5)	0.9191	22.00(8)	bcc	68.7	3.247(3)			17.12(8)
bct	17.1	3.6133(5)	3.3278(5)	0.9210	21.72(1)	bcc	70.0	3.241(3)			17.02(9)
bct	18.9	3.5941(5)	3.3179(4)	0.92317	21.43(1)	bcc	73.9	3.228(1)			16.81(4)
bct	19.2	3.5910(8)	3.3160(9)	0.92343	21.38(3)	bcc	78.6	3.216(3)			16.62(9)
bct	19.7	3.5853(5)	3.3126(4)	0.92394	21.29(1)	bcc	81.9	3.205(5)			16.5(1)
bct	20.8	3.5734(5)	3.3059(4)	0.92514	21.11(1)	bcc	85.9	3.191(5)			16.2(1)
bct	22.5	3.5579(5)	3.2969(5)	0.92666	20.87(1)	bcc	89.9	3.181(1)			16.09(4)
bct	24.0	3.5438(4)	3.2891(5)	0.92814	20.65(1)	bcc	93.3	3.171(1)			15.95(4)
bct	25.4	3.5319(4)	3.2823(5)	0.92934	20.47(1)	bcc	96.7	3.163(1)			15.82(4)
bct	26.7	3.5206(5)	3.2756(5)	0.93043	20.30(1)	bcc	99.9	3.1548(5)			15.70(2)
bct	28.3	3.5071(5)	3.2678(6)	0.93177	20.10(1)	bcc	102.9	3.1465(5)			15.58(1)
bct	29.2	3.4998(5)	3.2632(6)	0.93241	19.99(1)	bcc	106.4	3.1391(4)			15.47(1)
bct	30.9	3.4869(4)	3.2558(6)	0.93372	19.79(1)	bcc	109.8	3.1297(5)			15.33(2)
bct	31.5	3.4816(5)	3.2518(6)	0.93399	19.71(1)	bcc	113.9	3.1215(8)			15.21(3)
						bcc	117.6	3.114(1)			15.10(5)
						bcc	122.5	3.1056(4)			14.97(1)
						bcc	125.0	3.0995(3)			14.88(1)
						bcc	128.2	3.0935(4)			14.80(1)
						bcc	131.4	3.0862(4)			14.70(1)
						bcc	134.8	3.0797(5)			14.60(2)
						bcc	137.7	3.0749(4)			14.54(1)

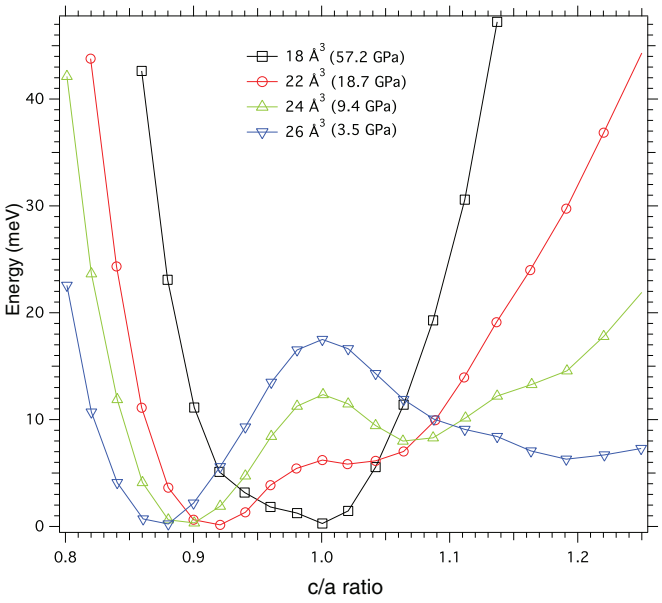

FIG. 7. (Color online) Variation in energy (meV) as a function of the c/a axial ratio for body-centered Sn with atomic volumes ranging between 26 and 18 Å, corresponding to pressures between $P = 3.5$ and 57.2 GPa.

(enthalpy) as a function of the c/a ratio at constant volume within the body-centered structures at $T = 0$ K. The results are shown between $V = 26$ Å^3, that corresponds to $P = 3.5$ GPa from the EOS obtained from constant P calculations, described below, and 18 Å^3, corresponding to $P = 57.2$ GPa (Fig. 7). Between 9.5 and 25 GPa, the minimum-energy structure exhibits a tetragonal (bct) distortion with a c/a value that increases from 0.90 to 0.93 as expected from experimental results. Above $P = 60$–70 GPa ($V < 18$ Å^3), the bcc structure results in the stable global minimum energy with an anharmonic potential that tends to become more symmetric as pressure increases.

At low pressure, a subsidiary minimum in the curve is present at $c/a = 1.08$, indicating the presence of a secondary metastable tetragonally distorted structure. The two are separated by a small barrier (12 meV) that is less than both 50% of kT at room temperature and the zero-point vibrational energy in the system ($\sim$20 meV), estimated from phonon density of states calculations and measurements.[40] This is an interesting observation that has a bearing on our interpretation of the structural distortions observed experimentally and on the thermal and mechanical properties of the system. As pressure is increased, the secondary minimum moves to smaller c/a values, its energy becomes lowered, and the barrier between the two minima is reduced. By 20 Å^3 ($P = 33.4$ GPa), the barrier has vanished entirely, resulting in a flat potential-energy curve with its minimum extending between $c/a = 0.93$ and 1.02 (Fig. 7). This result implies that the crystal is no longer mechanically stable against tetragonal lattice distortion in this pressure range. As the pressure is increased further, the potential steepens on both sides to form a slightly asymmetric minimum centered around the cubic (bcc) c/a value.

The picture that emerges from these DFT calculations is, thus, rather different from that suggested from the previous paper.[20] The possibility of an incipient first-order phase transition between stable and metastable structures with different c/a values only exists at the lowest pressures, and the metastable polymorph with larger c/a has a tetragonally distorted structure. We agree with the previous results that the bcc structure is stabilized at pressures greater than approximately 58 GPa, and this corresponds with the experimental result. However, the behavior in the intermediate ($P = 40$–70-GPa) range where both sets of bct and bcc reflections clearly coexist in the experimental diffraction patterns remains to be explained. One possible rationalization is that, within this range of volumes, the perfectly infinite single crystal, that is considered by the DFT calculations, has become mechanically unstable against c/a distortion. The flat potential-energy minimum does not permit this crystal to achieve a well-defined ground state so that the system may seek to minimize its free energy by spontaneous formation of domains with particular c/a values within the range. If such domains were sufficiently large, they could diffract x rays independently to give rise to apparently coexisting signatures of the bct and bcc phases. This model remains to be tested in future studies.

We carried out additional calculations of the energy as a function of c/a and b/a ratios for volumes extending throughout the range to explore the emergence of the orthorhombic (bco) distortion observed above 32 GPa. The results are shown as PES maps in the region of the global energy minimum (Fig. 8). We found that, at all pressures, the global minimum remained centered at $b/a = 1$ for both tetragonal and cubic solutions. However, the minimum-energy contours in the PES showed a strong diagonal slope, indicating that b/a distortions would be experienced for any slight deviation in the c/a value from the global minimum. Since the energies involved are very small (Fig. 8) and the potentials are highly anharmonic, b/a distortions on the order of 0.996 as determined experimentally can be experienced in response to vibrational excitation or if any small axial strains are present in the system studied experimentally. Those could occur due to any slight nonhydrostaticity in the pressurization environment or to the spontaneous appearance of nanoscale domains with a range of c/a values as suggested above.

C. Combining experimental and DFT points of view

The experiments clearly show the coexistence of the bco and bcc diffraction signatures occurring over a wide pressure range. That could be consistent with a first-order phase transition occurring between the two polymorphs, related by an energy barrier that leads to kinetic inhibition and metastable coexistence during room-temperature compression experiments. However, in the intermediate-pressure range, the volume of each phase could not be derived self-consistently from each of its diffraction lines, and the EOS could not be expressed simply as a weighted sum of the two bco and bcc contributions, indicating that lattice strains must be present in the system.

The DFT calculations did show evidence for two minimum-energy structures occurring at the lowest pressures, but these were different variants of the bct phase with c/a values either less than or greater than unity. As the pressure is increased towards the coexistence region, the barrier between the minima

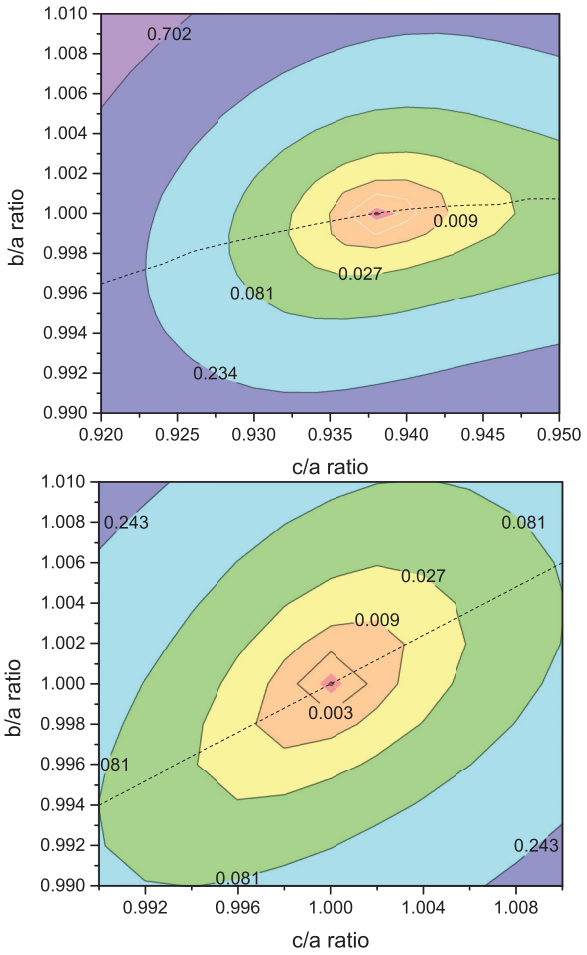

FIG. 8. (Color online) Two-dimensional plots of calculated enthalpy as a function of c/a and b/a ratios for body-centered Sn phases at $V = 20.0$ Å^3 (top) and $V = 18.5$ Å^3 (bottom), corresponding to pressures of 33.4 and 50.0 GPa. Contour labels are in meV/atom. The dashed line indicates the equilibrium b/a value as a function of c/a. When c/a is distorted away from the optimal value, a corresponding distortion will be induced in b/a, leading to orthorhombic (bco) structures.

disappears, and the structure assumes a mechanically unstable potential function where a wide range of c/a values, extending from 0.93 to 1.02, can be sampled without any energetic barrier. We propose that such a structure is likely to seek a minimum-energy solution by spontaneously developing locally strained lattice domains. Some of these will have $c/a = 1$, and the x-ray pattern could resemble that of coexisting bco and bcc macroscopic phases if the domain sizes are sufficiently large (i.e., on the order of a few nanometers or greater) to give rise to independent diffraction signatures. The resulting domains would be highly strained as observed experimentally. In this view, the structural coexistence range between 40 and 70 GPa is not due to an inherently first-order phase transition between bco and bcc polymorphs that could exist separately and potentially form a mechanical mixture but, instead, appears as a response of the system to a mechanical instability that causes it to seek a minimum free energy by developing nanoscopic domains. The polymorphic forms with different c/a ratios can, thus, not exist independently in the absence of an anisotropic stress field to which they respond readily because of the low barriers and spacing between energy contours existing within the potential-energy surface. The occurrence of the bct-bco distortion observed experimentally can be related to the same phenomena. The b/a ratio calculated for all tetragonal and cubic solutions remains centered at unity throughout the pressure range, but any small deviations in the c/a parameter from the ideal values will cause the appearance of an orthorhombic distortion. We suggest that this is observed during the compression experiments as the volume is reduced and slightly anisotropic stress-strain conditions are produced, either extrinsically from the PTM and intergrain contacts within the polycrystalline material or from spontaneous domain formation to relax the free energy of the crystalline system as it enters a regime of mechanical instability.

IV. CONCLUSION

We have carried out detailed experimental and theoretical experiments to study and to understand the unusual high-pressure polymorphism and structural transformations of Sn throughout the pressure range of 0–138 GPa. This element lies at a critical boundary among semiconducting and metallic behavior, localized vs extended bonding, and participation of d orbitals in its electronic manifold. The unusual structural and phase transformation behaviors are likely due to the electronic structure changes in this material as it is compressed. We experimentally observed the formation of a new orthorhombic polymorph from the bct phase above 32 GPa. That structure is rationalized by our DFT calculations as occurring due to c/a distortions away from the global energy minimum. Our experiments confirm the suggested coexistence of bco and bcc structures throughout a wide pressure range of 40–70 GPa. That behavior has been suggested to indicate a first-order phase transition between the two polymorphs. However, our DFT calculations indicate, instead, that the energy barrier between the stable and the metastable structures with different c/a ratios vanishes above approximately 33 GPa, resulting in a hypothetical material with no proper ground state subject to a wide range of axial distortions. We conclude that the material studied experimentally seeks to minimize its free energy by developing spontaneous domain structures with a range of c/a values, including bco and bcc solutions, that give rise to apparently independent diffraction signatures. These are obviously subject to localized axial strain fields as evidenced by the experimental data analysis. Our results suggest an interesting view of the properties of elemental metallic Sn subjected to pressures in the 30–70-GPa range. The material becomes mechanically soft due to the lowering or disappearance of energy barriers associated with axial strain, and we should expect that this will have an influence on phonon propagation as well as other thermal and mechanical properties.

ACKNOWLEDGMENTS

We acknowledge the European Synchrotron Radiation Facility for provision of the synchrotron radiation facilities. This work was partly supported by the Institute of Shock Physics initiated by a main award from AWE via a subcontract from Imperial College London.

*salamat@physics.harvard.edu
†p.f.mcmillan@ucl.ac.uk

[1]A. Hermann, J. Furthmüller, H. W. Gäggeler, and P. Schwerdtfeger, Phys. Rev. B **82**, 155116 (2010).
[2]H. Olijnyk and W. B. Holzapfel, J. Phys. **C8**, 153 (1984).
[3]M. I. McMahon, R. J. Nelmes, N. G. Wright, and D. R. Allan, Phys. Rev. B **50**, 739 (1994).
[4]R. J. Nelmes, H. Liu, S. A. Belmonte, J. S. Loveday, M. I. McMahon, D. R. Allan, D. Häusermann, and M. Hanfland, Phys. Rev. B **53**, 2907 (1996).
[5]M. Hanfland, U. Schwarz, K. Syassen, and K. Takemura, Phys. Rev. Lett. **82**, 1197 (1999).
[6]K. Takemura, U. Schwarz, K. Syassen, N. E. Christensen, M. Hanfland, D. L. Novikov, and I. Loa, Phys. Status Solidi B **223**, 385 (2001).
[7]C. A. Vanderborgh, Y. K. Vohra, H. Xia, and A. L. Ruoff, Phys. Rev. B **41**, 7338 (1990).
[8]A. Kuznetsov, V. Dmitriev, L. Dubrovinsky, V. Prakapenka, and H. P. Weber, Solid State Commun. **122**, 125 (2002).
[9]M. J. P. Musgrave, Proc. R. Soc. London, Ser. A **272**, 503 (1963).
[10]J. C. Jamieson (unpublished). Later referenced in Ref. 11.
[11]D. Barnett, V. Bean, and T. Hall, J. Appl. Phys. **37**, 875 (1966).
[12]M. Liu and L.-G. Lui, High Temp. - High Press. **18**, 79 (1986).
[13]S. Desgreniers, Y. K. Vohra, and A. L. Ruoff, Phys. Rev. B **39**, 10359 (1989).
[14]A. Salamat, G. Garbarino, A. Dewaele, P. Bouvier, S. Petitgirard, C. J. Pickard, P. F. McMillan, and M. Mezouar, Phys. Rev. B **84**, 140104 (2011).
[15]Y. Yao and D. D. Klug, Solid State Commun. **151**, 1873 (2011).
[16]R. Briggs, D. Daisenberger, A. Salamat, G. Garbarino, M. Mezouar, M. Wilson, and P. F. McMillan, J. Phys.: Conf. Ser. **377**, 012035 (2012).
[17]B. Schwager, M. Ross, S. Japel, and R. Boehler, J. Chem. Phys. **133**, 084501 (2010).
[18]S. T. Weir, M. J. Lipp, S. Falabella, G. Samudrala, and Y. K. Vohra, J. Appl. Phys. **111**, 123529 (2012).
[19]N. E. Christensen, Solid State Commun. **85**, 151 (1993).
[20]N. E. Christensen and M. Methfessel, Phys. Rev. B **48**, 5797 (1993).
[21]A. Dewaele, P. Loubeyre, and M. Mezouar, Phys. Rev. B **70**, 094112 (2004).
[22]P. I. Dorogokupets and A. R. Oganov, Phys. Rev. B **75**, 024115 (2007).
[23]A. P. Hammersley, S. O. Svensson, M. Hanfland, A. N. Fitch, and D. Häusermann, High Pressure Res. **14**, 235 (1996).
[24]R. Shirley, The CRYSFIRE system for automatic powder indexing (2006).
[25]K. Syassen, DATLAB, Version 1.37d (MPI/FKF, Stuttgart, Germany, 2005).
[26]B. H. Toby, J. Appl. Crystallogr. **34**, 210 (2001).
[27]S. J. Clark, M. D. Segal, C. J. Pickard, P. J. Hasnip, M. I. J. Probert, K. Refson, and M. C. Payne, Z. Kristallogr. **220**, 567 (2005).
[28]J. P. Perdew, K. Burke, and M. Ernzerhof, Phys. Rev. Lett. **77**, 3865 (1996).
[29]H. J. Monkhorst and D. J. Pack, Phys. Rev. B **13**, 5188 (1976).
[30]Y. Meng, D. J. Weidner, and Y. Fei, Geophys. Res. Lett. **20**, 1147 (1993).
[31]A. Dewaele and P. Loubeyre, High Press. Res. **27**, 419 (2007).
[32]S. Klotz, J.-C. Chervin, P. Munsch, and G. Le Marchand, J. Phys. D: Appl. Phys. **42**, 075413 (2009).
[33]J. Tempere and I. F. Silvera, J. Appl. Phys. **110**, 113523 (2011).
[34]K. Takemura and A. Dewaele, Phys. Rev. B **78**, 104119 (2008).
[35]F. Birch, Phys. Rev. **71**, 809 (1947).
[36]F. Birch, J. Geophys. Res. **37**, 227 (1952).
[37]F. Birch, J. Geophys. Res. **83**, 1257 (1978).
[38]F. D. Murnaghan, Proc. Natl. Acad. Sci. USA **30**, 244 (1944).
[39]R. Jeanloz, Geophys. Res. Lett. **8**, 1219 (2012).
[40]H. Giefers, E. A. Tanis, S. P. Rudin, C. Greeff, X. H. Ke, C. F. Chen, M. F. Nicol, M. Pravica, W. Pravica, J. Y. Zhao *et al.*, Phys. Rev. Lett. **98**, 245502 (2007).